

Influence of the scattering phase function on light transport measurements in turbid media performed with small source–detector separations

Judith R. Mourant, James Boyer, Andreas H. Hielscher, and Irving J. Bigio

Bioscience and Biotechnology Group CST-4, MS E535, Los Alamos National Laboratory, Los Alamos, New Mexico 87545

Received November 8, 1995

Many methods of optical tissue diagnosis require that measurements be performed with small source–detector separations in a backscatter geometry. Monte Carlo simulations are used to demonstrate that for these situations light transport depends on the exact form of the angular scattering probability distribution, $P(\theta)$. Simulations performed with different forms of $P(\theta)$ with the same value of $\langle \cos \theta \rangle$ result in the collection of significantly different fractions of the incident photons, particularly when small-numerical-aperture delivery and collection fibers are employed. More photons are collected for the distribution that has a higher probability of scattering events with $\theta > 125^\circ$. For the clinically relevant optical parameters employed here, the differences in light collection are $>60\%$.

Optical techniques for tissue diagnosis are currently being developed that offer significant advantages over standard biopsy or cytology techniques in terms of both patient care and medical costs.^{1–4} Many clinical applications require the use of an endoscope, and consequently many optical diagnostic methods employ fiber-optic probes. For endoscopic applications light delivery and collection fibers are in close proximity,^{5–7} or, in some cases, light delivery and collection are performed with the same fiber.⁸ It is important to understand the effects of various optical parameters on the collected signal in order to interpret these measurements appropriately. Tissue optical properties are typically characterized by the absorption coefficient μ_a , the scattering coefficient μ_s , and the angular scattering probability distribution (or phase function) $P(\theta)d\theta$ for scattering by an angle θ between $\theta + d\theta$ and θ . In this Letter we use Monte Carlo simulations to investigate the influence of the scattering phase function on the collected signal.

Frequently, modeling of photon transport in tissue is performed by use of the phenomenological Henyey–Greenstein (HG) phase function,^{9–11} which approximates angular scatter distributions calculated by Mie theory.¹² We have chosen to focus on how the phase function affects the collected signal, because to our knowledge this has not been done by other investigators and also because the appropriateness of using a HG phase function for these geometries has not been adequately demonstrated. Van Gemert *et al.* compared goniometer measurements of the stratum cornea and epidermis from $\sim 0^\circ$ to 60° with a HG phase function.¹³ Although the HG phase function fits the data reasonably well, there are differences in the shape of the experimental and theoretical curves of $P(\theta)\sin \theta$. Also, no data were presented for the higher scattering angles, which, as will be shown, are critical for some measurement geometries. Measurements of the scattering phase function of brain tissue have been made to almost 180° , which show an increase in scattering probability at

angles greater than 150° .¹⁴ Such an increase is not seen in HG phase functions.

Because there are differences between the HG phase function and experimentally measured phase functions, the question arises as to whether the HG function is an accurate enough expression for the phase function when the separation between light delivery and collection is small or if differences in the model and experimental phase functions can affect the collected signal. Therefore, we have performed simulations with two phase functions that have the same average value of the cosine of the scattering angle, $g = \int P(\theta)\cos \theta d\Omega$, but differ in probabilities of high-angle scattering events.

The geometry for the Monte Carlo simulations is shown in Fig. 1. Both fibers have the same numerical aperture, NA, and the same diameter, $2a = 200 \mu\text{m}$. The fibers are adjacent, such that the fiber center–center distance d is $200 \mu\text{m}$. This geometry is similar to those used in clinical tests of optical diagnostics in the esophagus, bladder, and cervix.^{6,7,15} The simulations were performed with NA's from 0.22 to 0.64.

We launch photons by choosing two random numbers to determine the point on the fiber face from which the photon is emitted. This point is specified by a radial distance and an azimuthal angle as in Eqs. (1)

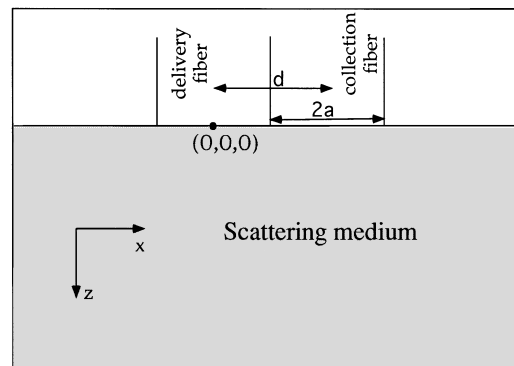


Fig. 1. Geometry for the Monte Carlo simulations.

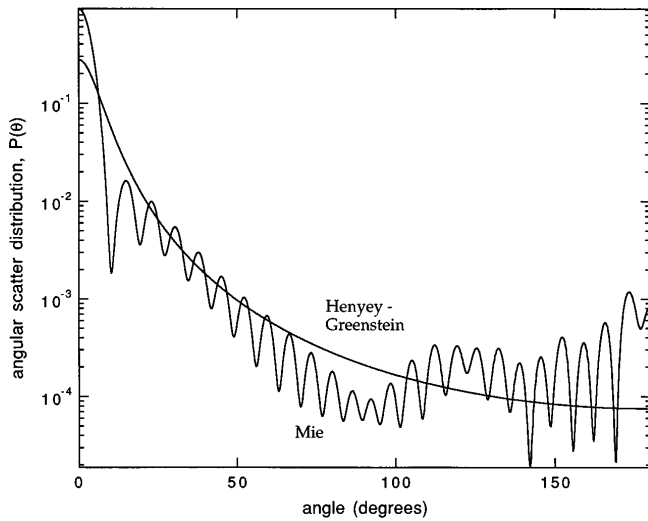


Fig. 2. Mie and HG phase functions used in the simulations. $g = 0.8786$ for both functions.

and (2) below, where ξ_i are random numbers. The deviation in the initial direction of travel from the z axis is defined by the polar angle, θ , in Eq. (3), where n_f is the index of the fiber and n_m is the index of the medium, and NA is the fiber NA. Equation (3) restricts θ to within limits set by the NA and takes into account Snell's law at the medium's surface. An azimuthal angle, $\Psi = 2\pi\xi_4$, is also needed to define the direction of travel:

$$r = a\sqrt{\xi_1}, \quad (1)$$

$$\Psi_f = 2\pi\xi_2, \quad (2)$$

$$\theta = [\sin^{-1}(NA n_f/n_m)]^* \xi_3. \quad (3)$$

Photon propagation is handled in the same general manner as described in Refs. 9 and 16. However, our implementation allows for either a HG phase function or a phase function computed from Mie theory. The implementation of a Mie phase function is based on calculation of a table of the cumulative distribution for the phase function $P(\theta)$ that can be sampled with a random number ξ . The Mie phase function and the corresponding HG phase function used in the simulations are shown in Fig. 2. The Mie calculations were performed for a polystyrene sphere in water at 600 nm. This results in values typical of tissue: $g = 0.8786$ and for a concentration of 1.04% spheres by weight $\mu_s = 100.6 \text{ cm}^{-1}$.

Photons are terminated from the simulation when they leave the surface of the medium or travel too far from the midpoint between the fibers. (Reflection at the surface is taken into account; Snell's law is used to calculate reflectance at the air-water and fiber-water interfaces.) Maxima for the depth and the radial distance from $(x = d/2, y = 0, z = 0)$ are set. We determined these values by running the simulation to find values for these cutoffs that had negligible effect on the simulation results. A photon is collected when it crosses $z = 0$ at a point under the collection fiber and when the angle between the z axis and the photon propagation direction in the fiber is less than

the limit defined by the NA of the fiber. For collected photons the number of times that a photon scattered through an angle θ as it traveled from the source to the collection fiber (weighted by the fraction of the photon that was collected) was recorded for 100 intervals of $\cos \theta$. This distribution, normalized according to Eq. (4), is referred to as $P_{\text{collected}}(\theta)$:

$$\int_0^\pi P_{\text{collected}}(\theta) \sin \theta d\theta = 1. \quad (4)$$

The fractions of photons collected, F_{HG} and F_{Mie} , using the Mie and HG phase functions, respectively, are plotted in Fig. 3 as a function of the fiber NA. For both values of absorption more photons were collected when the Mie phase function rather than the HG phase function was used. This can be explained by the greater probability of high-angle scattering events when the Mie phase function is employed.

In Fig. 4 the percent difference in the fraction of photons collected when a Mie phase function rather than a HG phase function is used, $100^*(F_{\text{Mie}} - F_{\text{HG}})/F_{\text{HG}}$, is plotted as a function of NA. Differences in the number of collected photons can be greater than 60% when a Mie phase function rather than a HG phase function is used. As NA increases, $100^*(F_{\text{Mie}} - F_{\text{HG}})/F_{\text{HG}}$ decreases. This is attributed to the fact that at higher NA's photons can exit and enter the fibers at larger angles, and therefore the change in direction between entering and leaving the media can be less than it is with low-NA fibers. Therefore, high-angle scattering events are not so necessary, and the differences between the Mie and HG phase functions are not so important for determining how many photons are collected for high-NA fibers as for low-NA fibers.

Based on Figs. 2 and 3, and 4(a) it seems likely that the collected photons undergo more high-angle scattering events than the average photon in the media. We have examined this phenomenon, and the

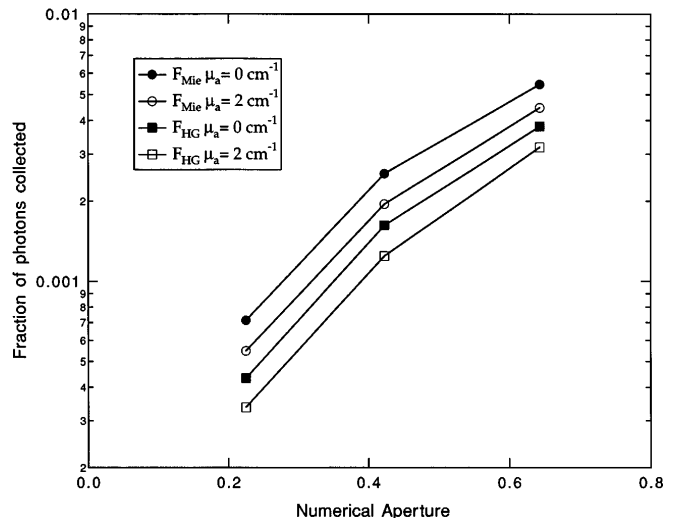


Fig. 3. Fraction of input photons collected as a function of NA for the HG (squares) and Mie (circles) phase functions. The optical parameters were $g = 0.8786$, $\mu_s = 100.6 \text{ cm}^{-1}$, and $\mu_a = 0 \text{ cm}^{-1}$ (filled symbols) or $\mu_a = 2 \text{ cm}^{-1}$ (open symbols). Errors are the same size as or smaller than the symbols.

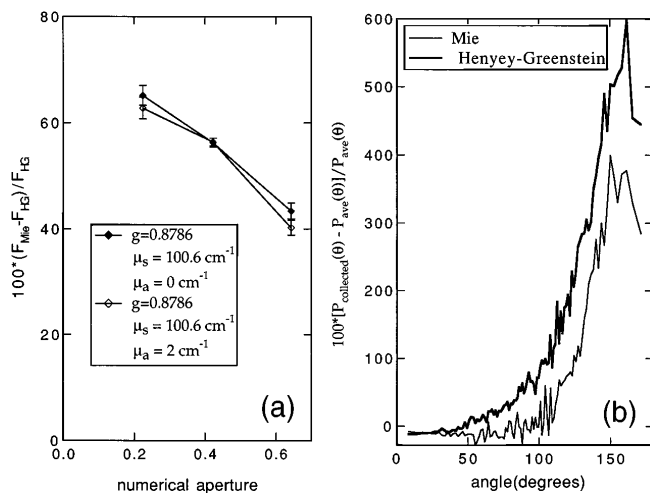


Fig. 4. Percent difference in the fraction of collected photons for the Mie phase function compared with the HG phase function. F_{Mie} and F_{HG} are the fractions of photons collected when the Mie and the HG phase functions are used, respectively. (b) The percent difference, $[P_{\text{collected}}(\theta) - P_{\text{ave}}(\theta)]^* 100 / P_{\text{ave}}(\theta)$, between the distribution of angles through which collected photons are scattered, $P_{\text{collected}}(\theta)$, and the distribution of angles through which the average photon in the media scatters, $P_{\text{ave}}(\theta)$. The calculations were performed with $\mu_s = 100.6 \text{ cm}^{-1}$, $\mu_a = 2 \text{ cm}^{-1}$, and NA = 0.42.

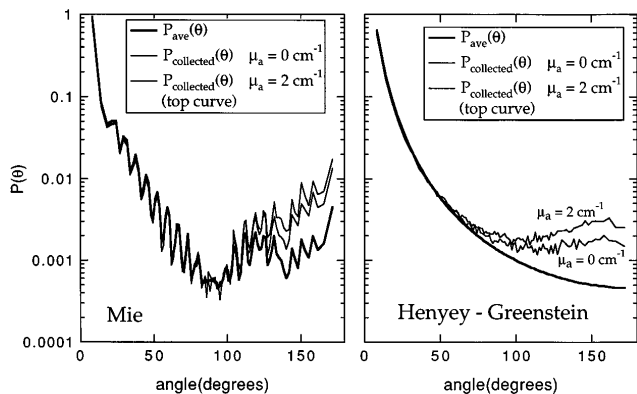


Fig. 5. Distribution of angles through which the average photon in the media scatters, $P_{\text{ave}}(\theta)$, and the distribution of angles, $P_{\text{collected}}(\theta)$, through which collected photons scattered. The optical parameters were $g = 0.8786$, $\mu_s = 100.6 \text{ cm}^{-1}$, and $\mu_a = 0 \text{ cm}^{-1}$ (middle curve) or $\mu_a = 2 \text{ cm}^{-1}$ (top curve).

results are shown in Figs. 4(b) and 5. $P_{\text{collected}}(\theta)$ is compared with $P_{\text{ave}}(\theta)$, the scattering probability function used in the Monte Carlo simulation. $P_{\text{ave}}(\theta)$ is also the scattering probability distribution of the average photon in the medium. The differences between $P_{\text{collected}}(\theta)$ and $P_{\text{ave}}(\theta)$ in Fig. 5 are greater for $\mu_a = 2 \text{ cm}^{-1}$ than for $\mu_a = 0 \text{ cm}^{-1}$. This likely is because long path lengths are less likely for larger μ_a ; therefore there are fewer scattering events, and the collected photons must undergo a higher fraction of large-angle scattering events for larger μ_a . Consistent with earlier results, the difference between $P_{\text{collected}}(\theta)$ and $P_{\text{ave}}(\theta)$ is greater when a HG phase

function rather than a Mie phase function is used, as shown in Fig. 4(b).

The results presented here are relevant to the development of optical tissue diagnostics. We have demonstrated that for source-detector separations typical of endoscopic applications, two phase functions having the same value of g but different shapes can give significantly different results in Monte Carlo simulations. The difference in the fraction of collected photons for the two phase functions is attributed to a higher probability of large-angle scattering events for the Mie phase function than with the HG phase function. The dependence of light collection on details of the angular scattering probability distribution is a function of the NA of the collection and delivery fibers. A strong dependence on details of high-angle scattering events may be more useful in some applications than others. Therefore the choice of fiber NA depends on the application.

References

1. N. Ramanujan, M. F. Mitchell, A. Mahadevan, S. Warren, S. Thomsen, E. Silva, and R. Richards-Kortum, Proc. Natl. Acad. Sci. USA **91**, 10193 (1994).
2. R. Richards-Kortum, R. P. Rava, R. E. Petras, M. Fitzmaurice, M. Sivak, and M. S. Feld, Photochem. Photobiol. **53**, 777 (1991).
3. J. J. Baraga, M. S. Field, and R. P. Rava, Proc. Natl. Acad. Sci. USA **89**, 3473 (1992).
4. S. Andersson-Engels, J. Johansson, K. Svanberg, and S. Svanberg, Proc. SPIE **1203**, 76 (1990).
5. R. M. Cothren, R. Richards-Kortum, M. V. Sivak, M. Fitzmaurice, R. P. Rava, G. A. Boyce, M. Doxtader, R. Blackman, T. B. Ivanc, G. B. Hayes, M. S. Feld, and R. E. Petras, Gastrointest. Endosc. **36**, 105 (1990).
6. T. Vo-Dinh, M. Panjehpour, B. F. Overholt, C. Farris, F. P. Buckley III, and R. Sneed, Lasers Surg. Med. **16**, 41 (1995).
7. J. R. Mourant, I. J. Bigio, J. Boyer, R. L. Conn, T. Johnson, and T. Shimada, Lasers Surg. Med. **17**, 350 (1995).
8. K. T. Schomacker, J. K. Frisoli, C. C. Compton, T. J. Flotte, J. M. Richter, N. S. Nishioka, and T. M. Deutsch, Lasers Surg. Med. **12**, 63 (1992).
9. S. L. Jacques and L. Wang, in *Optical-Thermal Response of Laser Irradiated Tissue*, A. J. Welch and M. J. C. van Gemert, eds. (Plenum, New York, 1995), pp. 73-100.
10. R. A. J. Groenhuis, H. A. Ferwerda, and J. J. Ten Bosch, Appl. Opt. **22**, 2456 (1983).
11. S. T. Flock, M. S. Patterson, B. C. Wilson, and D. R. Wyman, IEEE Trans. Biomed. Eng. **36**, 1162 (1989).
12. L. G. Henyey and J. L. Greenstein, Astrophys. J. **93**, 70 (1941).
13. M. J. C. van Gemert, S. L. Jacques, H. J. C. M. Sterenborg, and W. M. Star, IEEE Trans. Biomed Eng. **36**, 1146 (1989).
14. P. van der Zee, M. Essenpreis, and D. T. Delpy, Proc. SPIE **1888**, 454 (1993).
15. N. Ramanujam, M. F. Mitchell, A. Mahadevan, S. Thomsen, E. Silva, and R. Richards-Kortum, Gynecol. Oncol. **52**, 31 (1994).
16. L. H. Wang, S. L. Jacques, and L. Zheng, Comput. Meth. Programs Biomed. **47**, 131 (1995).